

# Equilibria, Stability, and Sensitivity for the Aerial Suspended Beam Robotic System subject to Model Uncertainty

C. Gabellieri<sup>1</sup> *IEEE Member*, M. Tognon<sup>2</sup> *IEEE Member*, D. Sanalidro<sup>3</sup> *IEEE Member*, A. Franchi<sup>1,3</sup>, *IEEE Senior Member*

**Abstract**—This work studies how parametric uncertainties affect the cooperative manipulation of a cable-suspended beam-shaped load by means of two aerial robots not explicitly communicating with each other. In particular, the work sheds light on the impact of the uncertain knowledge of the model parameters available to an established communication-less force-based controller. First, we find the closed-loop equilibrium configurations in the presence of the aforementioned uncertainties, and then we study their stability. Hence, we show the fundamental role played in the robustness of the load attitude control by the internal force induced in the manipulated object by non-vertical cables. Furthermore, we formally study the sensitivity of the attitude error to such parametric variations, and we provide a method to act on the load position error in the presence of the uncertainties. Eventually, we validate the results through an extensive set of numerical tests in a realistic simulation environment including underactuated aerial vehicles and sagging-prone cables.

*Index Terms*—...

## I. INTRODUCTION

IT is nowadays universally acknowledged that the interest in Unmanned Aerial Vehicles (UAVs) is becoming wider and wider by virtue of their ability to embrace an ample set of applications. A very recent and popular topic in aerial robotics is physical interaction using aerial manipulators [1], [2], [3] for applications such as contact-based inspection, assembly, human assistance, etc. To solve these challenges, aerial platforms are endowed with physical interaction tools, such as cables [4] or more complex robotic arms [5].

Researchers have considered taking advantage of the cooperation between multiple robots to enhance the overall payload and manipulate large objects [6], [7], [8], [9]. Different methods have been developed to tackle multi-robot aerial manipulation. In [10] and [11] the authors use passive manipulation tools to solve the cooperative aerial transportation of rigid and elastic objects, respectively. Multiple flying arms are instead used in [12], [13]. Cables have been often considered in multi-robot manipulation scenarios, because, in addition to being lightweight and low-cost, they also mitigate the coupling between the system dynamics and the robots’

attitude, which can simplify the control problem, especially when using underactuated aerial platforms.

### A. Related Works

The problem of manipulating a cable-suspended load through a team of aerial vehicles has been studied, e.g., in [14], [15], [16], [17], [18], [19]. In [20], a robust pose controller for a cable-suspended load manipulated by multiple UAVs is presented. Stability is ensured through gain tuning given a bound on the uncertainties affecting the kinematic parameters. Formation control to transport the payload with a focus on robustness is described in [21], where modeling uncertainties are also taken into account.

A standard system that has attracted substantial interest in the research community is composed of *two* aerial vehicles manipulating a *beam-like load* through cables [22], [23], [24], [17], [25], [26], [27]. Such standard configuration is of interest for several real-world applications, especially in the construction field, where we find columns, wooden pillars, iron beams for cement walls, scaffolds, pipes, pieces of roofs, and other beam-like building elements. Two is the minimum number of aerial robots allowing to control both the position and attitude of a cable-suspended beam-like load [23]. While three aerial robots allow controlling the entire pose of a generic rigid body [28], using more than two robots for a beam-like load it is arguably not the optimal solution in most of the cases because of the increased complexity of the system without being necessary for the control of the load.

In [23], the authors propose a method for the transportation of a cable-suspended beam load by two aerial vehicles that have access to the state of the load. For both robots’ controllers, an integral term is added in the vertical direction to compensate for the error that would result from a lack of perfect knowledge of the load’s mass. In [24], centralized and decentralized model predictive control is proposed for a system of two UAVs manipulating a beam load through cables.

Decentralized algorithms as [29] are more robust and scalable with respect to (w.r.t.) the number of robots. However, because communication delays and packet losses are one of the principal causes undermining the performance and stability of the system in a real implementation, and because the hardware and software complexity can be reduced by confining explicit communication, decentralized *communication-less* approaches have been also intensively studied in the literature. In [26]

This work has been partially funded by the European Union’s Horizon Europe research and innovation program [grant agreement No. ID: 101059875] Flyfic and Horizon 2020 research and innovation programme [grant agreement No. 871479] AERIAL-CORE.

<sup>1</sup>Robotics and Mechatronics group, EEMCS faculty, University of Twente, Enschede, The Netherlands <sup>2</sup>Inria, Univ Rennes, CNRS, IRISA, Campus de Beaulieu, 35042 Rennes Cedex, France <sup>3</sup>LAAS-CNRS, Université de Toulouse, CNRS, Toulouse, France. Email: a.franchi@utwente.nl

a method relying on visual feedback is presented. In alternative to vision, the other state-of-the-art approach usually employed to solve communication-less aerial manipulation of cable-suspended objects is a force-based method that uses admittance controllers and a leader-follower scheme [25], [30], [31], [32]. In this approach, the leader steers the system by tracking a trajectory, and the other robot, while sustaining part of the weight of the load, follows the leader by sensing a variation in the cable force.

A primary goal of [25] is to keep the cables always vertical during transportation, meaning that no internal force is induced in the object. The authors in [30] extend the results of [25] towards the  $N$ -robot case and provides a method for tuning the gains of the robot admittance controllers in order to improve the robustness against disturbances induced by unmodeled dynamics and parametric uncertainties. In both works experiments are shown in which, however, the altitude of the robots is set to a predetermined reference, allowing for only limited movements of the robots in the vertical direction or for a centralized movement coordination in the vertical direction.

For such popular class of communication-less, admittance-controlled, and leader-follower schemes, the formal analysis of the closed-loop system equilibrium configurations and their stability was presented for the first time in our previous work [31]. There, we have shown that to achieve full-pose regulation of the slung load, it is necessary to induce an internal force on the load through non-vertical cables, especially to prevent arbitrary movements of the robots in the vertical direction, which would perturb the regulation of the load pitch and center position. In [32], we considered  $N$  robots, empirically showing through extensive simulations the effect of changing the number of leader robots on the stability and robustness against disturbances. Both works tackle only the ideal case where perfect knowledge of the system parameters is available to the admittance controllers of each aerial robot.

Understanding if and how the uncertainties that are unavoidable in practice impact the pose regulation has been unknown until now, despite being of primary interest. Such a gap is filled in this work by introducing uncertainties on those system parameters used in the control action. In this work, we have discovered that the internal force induced by non-vertical cables plays a fundamental role in enabling task execution, especially in realistic conditions characterized by uncertainties. The importance of this is masked when vertical movements of the robots are prevented or anyway the leader-follower approach is used solely to regulate the load motion on the horizontal plane, as in [25], [30]. On the other hand, the role of the internal force is crucial if the admittance-based communication-less approach is applied in the full 3D space and, hence, communication-less full-pose regulation is sought.

### B. Contributions of the Work and Outline of the Paper

The contribution of this work is showing the effects of in-practice-unavoidable parametric uncertainties on the regulation of the load pose when the usual approach [25], [30], [31], [32] based on admittance-controlled leader-follower aerial robots

is used to manipulate a cable-suspended beam load in the absence of explicit communication. We address the problem aiming at a mathematically-sound point of view: after formally studying the equilibrium configurations of the closed-loop system in presence of uncertain parameters, we prove their stability using Lyapunov's theory.

Throughout the manuscript, we show that the intuitive idea of having the cables vertical is actually to be avoided when performing the manipulation with force-based methods in reality, i.e., when uncertainties are present. Specifically, we prove that the sole equilibrium configurations of the uncertain system when the cables are kept vertical and thus no internal force is induced in the object are highly undesirable ones. We formally investigate the impact of an internal force induced by non-vertical cables on the *robustness* of the load pose control. In addition, we show that the internal force diminishes the *sensitivity* of the load attitude error to parametric or uncertainty variations. We also present a method for correcting the load position inaccuracy induced by the uncertainties. Eventually, we present extensive numerical results supporting the claims conveyed by the theoretical analysis.

Last but not least, this work generalizes the system model by considering a generic position of the CoM of the load rather than assuming it to be exactly centered in the middle of the two anchoring points of the cables as done in [31].

The paper is organized as follows. Sec II contains some background useful to better understand the results of the work. In Secs III to V, we present the three main contributions of the work: Sec III contains the derivation of the equilibrium points, and Sec IV their stability analysis; Sec V highlights the role of the internal forces in the load error robustness and sensitivity to parametric variations. The results of the simulations and conclusive discussions are presented in Sec VI and Sec VII, respectively.

## II. BACKGROUND

In this section, we provide the background needed to understand the contribution of the work. Specifically, we quickly recall the system main variables, the dynamics equations, and the previously known results.

The considered system, schematically shown in Fig. 1, is the typical rigid beam-like load attached to two aerial vehicles by means of cables. The beam-like load has mass  $m_L \in \mathbb{R}_{>0}$  and positive-definite rotational inertia  $\mathbf{J}_L \in \mathbb{R}^{3 \times 3}$ . The frame  $\mathcal{F}_L = \{O_L, \mathbf{x}_L, \mathbf{y}_L, \mathbf{z}_L\}$ , where  $O_L$  coincides with the load CoM, is rigidly attached to the load. The inertial frame is denoted with  $\mathcal{F}_W = \{O_W, \mathbf{x}_W, \mathbf{y}_W, \mathbf{z}_W\}$  where  $\mathbf{z}_W$  is oriented in the direction opposite to the gravity. The position and orientation of  $\mathcal{F}_L$  w.r.t.  $\mathcal{F}_W$ , defined by the vector<sup>1</sup>  ${}^W\mathbf{p}_L \in \mathbb{R}^3$  and the rotation matrix  ${}^W\mathbf{R}_L \in SO(3)$ , respectively, describe the full configuration of the load. We recall that the rotation along the axis that passes between the two cable anchoring points is not controllable by the robots. Being the load a beam, only the yaw angle,  $\psi$ , and pitch angle,  $\theta$ , are sufficient

<sup>1</sup>The left superscript indicates the reference frame.

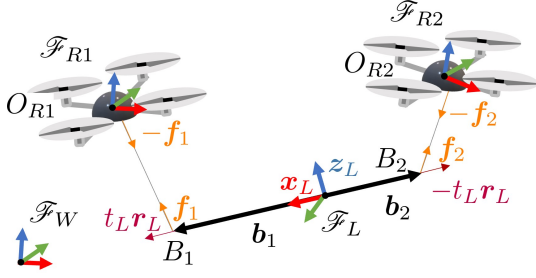


Fig. 1: Representation of the system and its major variables. The two aerial vehicles do not need to be necessarily quadrotors since the analysis and control design is valid for general aerial vehicles.

to describe the attitude. The usual Newton-Euler equations describe the dynamics of the load:

$$\begin{aligned} m_L \ddot{\mathbf{p}}_L &= -m_L g \mathbf{e}_3 + \mathbf{f}_e \\ \dot{\mathbf{R}}_L &= \mathbf{S}(\boldsymbol{\omega}_L) \mathbf{R}_L \\ \mathbf{J}_L \dot{\boldsymbol{\omega}}_L &= -\mathbf{S}(\boldsymbol{\omega}_L) \mathbf{J}_L \boldsymbol{\omega}_L - \mathbf{B}_L \boldsymbol{\omega}_L + \boldsymbol{\tau}_e, \end{aligned} \quad (1)$$

where  $\boldsymbol{\omega}_L \in \mathbb{R}^3$  is the angular velocity of  $\mathcal{F}_L$  w.r.t.  $\mathcal{F}_W$  expressed in  $\mathcal{F}_L$ ,  $\mathbf{S}(\star)$  is the *skew operator*<sup>2</sup>,  $g$  is the gravitational acceleration,  $\mathbf{e}_i$  is the canonical unit vector with a 1 in the  $i$ -th entry,  $\mathbf{f}_e \in \mathbb{R}^3$  and  $\boldsymbol{\tau}_e \in \mathbb{R}^3$  are the sum of external forces and torques acting on the load, respectively. An energy dissipation phenomenon is modeled by a damping factor defined by the positive definite matrix  $\mathbf{B}_L \in \mathbb{R}^{3 \times 3}$ .

The load is suspended by two cables from two anchoring points,  $B_i$  with  $i = 1, 2$ , for which the position w.r.t.  $\mathcal{F}_L$  is described by the vector  ${}^L\mathbf{b}_i \in \mathbb{R}^3$ . By simple kinematics, the position of  $B_i$  w.r.t.  $\mathcal{F}_W$  is then given by  $\mathbf{b}_i = \mathbf{p}_L + \mathbf{R}_L {}^L\mathbf{b}_i$ . Since we are considering a beam-like load, the object CoM is aligned with the two anchoring points of the cables. Without loss of generality, we assume that  ${}^L\mathbf{b}_1 = [b_1 \ 0 \ 0]^\top$  and  ${}^L\mathbf{b}_2 = [-b_2 \ 0 \ 0]^\top$ , where  $b_i \in \mathbb{R}_{>0}$ , for  $i = 1, 2$ . We also define the beam's length  $L = b_1 + b_2$ . The  $i$ -th cable is rigidly attached to the  $i$ -th aerial vehicle at the point  $O_{Ri}$ . Centered in this point, we define a frame  $\mathcal{F}_{Ri} = \{O_{Ri}, \mathbf{x}_{Ri}, \mathbf{y}_{Ri}, \mathbf{z}_{Ri}\}$  rigidly attached to the vehicle.  $\mathcal{F}_{Ri}$  is used to describe the position and rotation of the vehicle w.r.t.  $\mathcal{F}_W$ , denoted by the vector  $\mathbf{p}_{Ri} \in \mathbb{R}^3$ , and the rotation matrix  $\mathbf{R}_{Ri} \in SO(3)$ , respectively. We define  $\mathbf{q}_R = [\mathbf{p}_{R1}^\top \ \mathbf{p}_{R2}^\top]^\top$ .

The use of recent robust controllers for unidirectional- and multidirectional-thrust vehicles [33], [34] and disturbance observers for aerial vehicles has been experimentally proven to result in negligible tracking errors even in the presence of external disturbances. Thanks to this fact, closed-loop translational dynamics of the robot subject to the position controller is 'de facto' equivalent to the one of a double integrator:  $\dot{\mathbf{p}}_{Ri} = \mathbf{u}_{Ri}$ , where  $\mathbf{u}_{Ri}$  is a virtual input. In other words, it is safe to assume that the aerial robots together with a sufficiently accurate position controller can track any desired  $C^2$  trajectory with negligible error in the domain of interest, independently from external disturbances [31]. In this work, we follow such experimentally validated common practice for the theoretical derivations in Secs III, IV, and V, while

<sup>2</sup>Given  $\mathbf{x} \in \mathbb{R}^3$ ,  $\mathbf{S}(\mathbf{x}) \in \mathbb{R}^{3 \times 3}$  is such that  $\mathbf{S}(\mathbf{x})\mathbf{y} = \mathbf{x} \times \mathbf{y}$  for all  $\mathbf{y} \in \mathbb{R}^3$ .

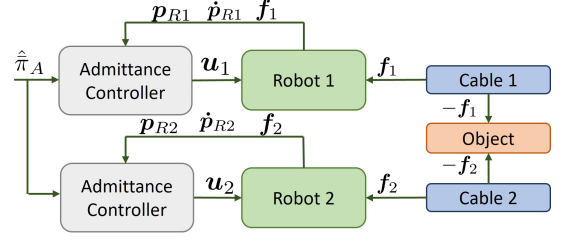


Fig. 2: Schematic representation of the overall system including both physical and control blocks. The input of the admittance controller is affected by the uncertainty of the system parameters.

we make use of a full quadrotor model for the numerical validation of Sec VI.

Cable-to-robot and cable-to-load connections are modeled as passive and mass-negligible rotational joints. Besides, the  $i$ -th cable is represented as a unilateral spring along its principal direction, which is a frequently adopted model [35], [31], [36], [37]. As commonly done in the state of the art, the cables' mass and inertia are assumed negligible in comparison the robots' and load's. Its parameters are the constant elastic coefficient  $k_i \in \mathbb{R}_{>0}$  and the constant rest length denoted by  $l_{0i}$ .

The attitude of the  $i$ -th cable w.r.t.  $\mathcal{F}_W$  by the normalized vector is<sup>3</sup>  $\mathbf{n}_i = \mathbf{l}_i / \|\mathbf{l}_i\| \in \mathbb{S}^2$ , where  $\mathbf{l}_i = \mathbf{p}_{Ri} - \mathbf{b}_i$ . The force acting on the load at  $B_i$ , given a certain length  $\|\mathbf{l}_i\|$  of the cable, is given by the simplified Hooke's law:

$$\mathbf{f}_i = t_i \mathbf{n}_i, \quad t_i = \begin{cases} k_i (\|\mathbf{l}_i\| - l_{0i}) & \text{if } \|\mathbf{l}_i\| - l_{0i} > 0 \\ 0 & \text{otherwise} \end{cases} \quad (2)$$

where  $t_i \in \mathbb{R}_{\geq 0}$  denotes the tension along the cable. The force produced on the other hand of the cable, i.e., on the  $i$ -th robot at  $O_{Ri}$ , is equal to  $-\mathbf{f}_i$ .

Combining equations (1)-(2), the dynamic model of the full system is:

$$\begin{aligned} \dot{\mathbf{v}}_R &= \mathbf{u}_R \\ \dot{\mathbf{v}}_L &= \mathbf{M}_L^{-1} (-c_L(\mathbf{v}_L) - g_L + G(\mathbf{q}_L)\mathbf{f}), \end{aligned} \quad (3)$$

where  $\mathbf{q}_L = (\mathbf{p}_L, \mathbf{R}_L)$ ;  $\mathbf{v}_R = [\dot{\mathbf{p}}_{R1}^\top \ \dot{\mathbf{p}}_{R2}^\top]^\top$ ;  $\mathbf{v}_L = [\dot{\mathbf{p}}_L^\top \ \boldsymbol{\omega}_L^\top]^\top$ ;  $\mathbf{u}_R = [\mathbf{u}_{R1}^\top \ \mathbf{u}_{R2}^\top]^\top$ ;  $\mathbf{f} = [\mathbf{f}_1^\top \ \mathbf{f}_2^\top]^\top$  where  $\mathbf{f}_i$  is given in (2) and is a function of the state;  $\mathbf{M}_L = \text{diag}(m_L \mathbf{I}_3, \mathbf{J}_L)$  with  $\mathbf{I}_3 \in \mathbb{R}^{3 \times 3}$  the identity matrix;  $g_L = [m_L g \mathbf{e}_3^\top \ 0]^\top$ ;

$$c_L = \begin{bmatrix} 0 \\ \mathbf{S}(\boldsymbol{\omega}_L) \mathbf{J}_L \boldsymbol{\omega}_L - \mathbf{B}_L \boldsymbol{\omega}_L \end{bmatrix}$$

and

$$G = \begin{bmatrix} \mathbf{I}_3 & \mathbf{I}_3 \\ \mathbf{S}({}^L\mathbf{b}_1) \mathbf{R}_L^\top & \mathbf{S}({}^L\mathbf{b}_2) \mathbf{R}_L^\top \end{bmatrix}$$

The two dynamics in (3) are coupled through the cable forces in (2).

We recall that, to regulate the pose of the transported load to a desired equilibrium  $\bar{\mathbf{q}}_L = (\bar{\mathbf{p}}_L, \bar{\mathbf{R}}_L)$ , an admittance controller is used on the robots [31]:

$$\mathbf{u}_{Ri} = \mathbf{M}_{Ai}^{-1} (-\mathbf{B}_{Ai} \dot{\mathbf{p}}_{Ri} - \mathbf{K}_{Ai} \mathbf{p}_{Ri} - \mathbf{f}_i + \boldsymbol{\pi}_{Ai}), \quad (4)$$

<sup>3</sup> $\mathbb{S}^2 = \{\mathbf{v} \in \mathbb{R}^3 \mid \|\mathbf{v}\| = 1\}$

where the positive-definite symmetric matrices  $M_{Ai}, B_{Ai}, K_{Ai} \in \mathbb{R}^{3 \times 3}$  are, respectively, the virtual inertia of the robot, and the damping and stiffness coefficients of a virtual spring-damper system that links the robot and a desired reference position, as it will be clearer in the following;  $f_i$  is the force exerted by the robot's own cable;  $\pi_{Ai} \in \mathbb{R}^3$  is an additional forcing input that properly set to steer the load to the desired configuration.

**Remark 1.** One can notice that (4) requires only local information: the state of the robot ( $p_{Ri}, \dot{p}_{Ri}$ ), which can be retrieved with standard onboard sensors like IMU, GPS, and cameras; the force applied by the cable,  $f_i$ , which can be directly measured by an onboard force sensor or estimated by a sufficiently precise model-based observer as done in [38], [25]. Therefore, the described method is decentralized and does not require explicit communication between the robots. However, it is interesting to see that the communication is not completely missing; rather, it is implicit. Indeed, the interaction forces between the robots and the load, via the cables, enable a kind of “physical” communication.

From equations (3) and (4), the closed-loop system dynamics can be written as  $\dot{v} = m(q, v, \pi_A)$  where

$$m(q, v, \pi_A) = \begin{bmatrix} M_A^{-1}(-B_A v_R - K_A q_R - f + \pi_A) \\ M_L^{-1}(-c_L(v_L) - g_L + Gf) \end{bmatrix}, \quad (5)$$

with  $q = (q_R, q_L)$ ,  $v = [v_R^\top v_L^\top]^\top$  and  $\pi_A = [\pi_{A1}^\top \pi_{A2}^\top]^\top$ . Furthermore  $M_A = \text{diag}(M_{A1}, M_{A2})$ ,  $B_A = \text{diag}(B_{A1}, B_{A2})$  and  $K_A = \text{diag}(K_{A1}, K_{A2})$ .

In order to coordinate the motion of the robots in a decentralized way, a *leader-follower* approach is used. In this way, only the designated leader will have an active control on the position of the load. On the other hand, the other robot will follow, partially sustaining the weight of the load and contributing to the control of the load attitude. Choosing without loss of generality, robot 1 as leader and robot 2 as follower, the leader-follower approach is achieved as usual [25], [30], [31], [32] by setting  $K_{A1} \neq 0$  and  $K_{A2} = 0$ .

**Definition 1** (Equilibrium configuration).  $q$  is an equilibrium configuration, indicated as  $\bar{q}_L$ , if  $\exists \pi_A$  s.t.  $0 = m(q, 0, \pi_A)$ , i.e., if the corresponding zero-velocity state is a forced equilibrium for the system (5) for a certain forcing input  $\pi_A$ .

**Definition 2** (Load internal force). For the considered system, given the vector of forces at the equilibrium,  $f$ , the load internal force is defined as

$$t_L := \frac{1}{2} f^\top [I_3 - I_3]^\top R_L e_1 =: \frac{1}{2} f^\top r_L, \quad (6)$$

where  $r_L = [I_3 - I_3]^\top \bar{R}_L e_1$ . We have that

- if  $t_L > 0$  the internal force causes a tension in the load;
- if  $t_L < 0$  the internal force causes a compression in the load.

The following result, proven in [31], provides the expression of the forcing input  $\pi_A$  and the robot configurations  $q_R$  for which, given a desired load configuration  $\bar{q}_L$ ,  $q = (q_R, \bar{q}_L)$  is an equilibrium configuration of the system.

**Theorem 1** (equilibrium inverse problem, provided in [31], reported here for completeness). Consider the closed-loop system (5) and assume that the load is at a given desired configuration  $\bar{q}_L = (\bar{p}_L, \bar{R}_L)$ . For each internal force  $t_L \in \mathbb{R}$ , there exists a unique constant value of the forcing input  $\pi_A = \bar{\pi}_A$  (and a unique position of the robots  $q_R = \bar{q}_R$ ) such that  $\bar{q} = (\bar{q}_L, \bar{q}_R)$  is an equilibrium of the system.

In particular  $\bar{\pi}_A$  and  $\bar{q}_R = [\bar{p}_{R1}^\top \bar{p}_{R2}^\top]^\top$  are given by

$$\bar{\pi}_A(\bar{q}_L, t_L) = K_A \bar{q}_R + \bar{f}(\bar{q}_L, t_L) \quad (7)$$

$$\bar{p}_{Ri}(\bar{q}_L, t_L) = \bar{p}_L + \bar{R}_L^L b_i + \left( \frac{\|\bar{f}_i\|}{k_i} + l_{0i} \right) \frac{\bar{f}_i}{\|\bar{f}_i\|}, \quad (8)$$

for  $i = 1, 2$ , where

$$\bar{f}(\bar{q}_L, t_L) = \begin{bmatrix} \bar{f}_1 \\ \bar{f}_2 \end{bmatrix} = \begin{bmatrix} \frac{b_2 m_L g}{L} \\ \frac{b_1 m_L g}{L} \end{bmatrix} \begin{bmatrix} I_3 \\ I_3 \end{bmatrix} e_3 + t_L \begin{bmatrix} I_3 \\ -I_3 \end{bmatrix} \bar{R}_L e_1. \quad (9)$$

From (7), we can see that the forcing input is made up of two parts: one that depends on the robots' positions computed from the load equilibrium configuration according to kinematic relations, and the other that depends on the equilibrium forces. The equilibrium forces are composed, according to (9), by one term that compensates gravity and one term that produces an internal force on the load of intensity  $t_L$ . We already know from [31] that, if  $\bar{\pi}_A$  is exactly applied to the closed-loop system (5),  $\bar{q}_L$  is an isolated load equilibrium configuration if  $t_L \neq 0$ , which is asymptotically stable if  $t_L > 0$  and unstable if  $t_L < 0$ . Instead,  $\bar{q}_L$  belongs to a continuum of equilibrium points containing any possible attitude of the load if  $t_L = 0$ .

### III. EQUILIBRIA UNDER UNCERTAINTY

In reality,  $\bar{\pi}_A$  in (7) cannot be applied exactly because of parametric uncertainties. Instead, one can apply only a version of  $\bar{\pi}_A$ , denoted with  $\hat{\pi}_A$ , computed using the nominal, uncertain values of the system parameters, (see Fig. 2 for a schematic representation of the control scheme with the nominal forcing input). In the following, if not differently stated, we consider the general case in which a whole set of uncertainties are present. These uncertainties affect the control law (7) and, in turn, affect the system equilibrium configurations. The uncertainties are the following:

- $m_L$  is unknown, but only its nominal value  $\hat{m}_L$  is available for the control design. We define the corresponding uncertainty as  $\Delta_m = m_L - \hat{m}_L$ ;
- $b_1$  is not known, but only its nominal value  $\hat{b}_1$  is available. The corresponding uncertainty, affecting the load CoM position, is  $\Delta_b = b_1 - \hat{b}_1$ ;
- $L$  is not known, but only its nominal value  $\hat{L}$  is available, and we define  $\Delta_\ell = \frac{1}{L} - \frac{1}{\hat{L}} = \ell - \hat{\ell}$  and  $\Delta_L = L - \hat{L}$ ;
- the model of the cable  $i$ -th is inexact. Therefore, the nominal length  $l_{0i}$  and stiffness  $k_i$  are not known, but only their nominal values  $\hat{l}_{0i}$  and  $\hat{k}_i$  are available for the control design. We define the uncertainties  $\Delta_{ki} = k_i - \hat{k}_i$ ,  $\Delta_{l_{0i}} = l_{0i} - \hat{l}_{0i}$ .

Note that the nominal value of  $b_2$ ,  $\hat{b}_2$ , depends on the previously defined quantities according to the relationship  $\hat{b}_2 = \hat{L} - \hat{b}_1$ . However, for convenience, we also define  $\Delta_{b2} = b_2 - \hat{b}_2$ .

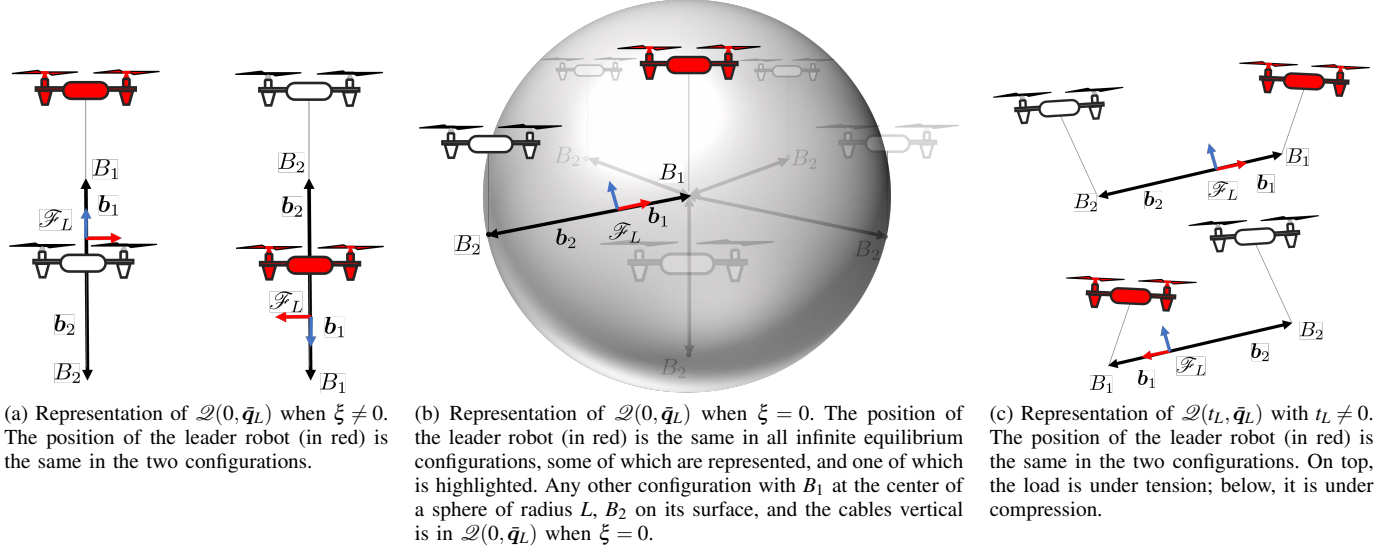


Fig. 3: Representation of the different equilibrium configurations of the system depending on  $t_L$  and  $\xi$ .

We shall now study the system's equilibrium configurations when  $\hat{\pi}_A$  is applied.

**Theorem 2** (equilibrium direct problem). *Given a desired load configuration  $\bar{q}_L = (\bar{p}_L, \bar{R}_L)$  and the internal force  $t_L \in \mathbb{R}$ , assume that the forcing input  $\hat{\pi}_A$  is computed from (7) and is applied to the closed-loop system (5). Then, the equilibrium configurations are all and only the ones satisfying the following conditions:*

$$p_{R1} = \hat{p}_{R1} - K_{A1}^{-1}(\Delta_m g e_3) := p_{R1}^{eq} \quad (10)$$

$$R_L := R_L^{eq} \text{ s.t. } S(e_1) R_L^{eq \top} \left[ \left( b_1 m_L - \frac{\hat{b}_1 \hat{m}_L L}{\hat{L}} \right) g e_3 + L t_L \bar{R}_L e_1 \right] = 0 \quad (11)$$

$$f_1 = m_L g e_3 - \frac{\hat{m}_L \hat{b}_1 g}{\hat{L}} e_3 + t_L \bar{R}_L e_1 := f_1^{eq} \quad (12)$$

$$f_2 = \frac{\hat{b}_1 \hat{m}_L g}{\hat{L}} e_3 - t_L \bar{R}_L e_1 = \hat{f}_2 := f_2^{eq} \quad (13)$$

$$p_L = p_{R1}^{eq} - R_L^{eq} b_1 - \left( \frac{\|f_1^{eq}\|}{k_1} + l_{01} \right) \frac{f_1^{eq}}{\|f_1^{eq}\|} := p_L^{eq}, \quad (14)$$

where  $\hat{p}_{R1}$  indicates the reference position of the leader robot computed as in (8), namely starting from  $\bar{p}_L, \bar{R}_L$ , but using the uncertain parameters.

*Proof.*  $\hat{\pi}_A$  is defined according to (7), where (9) becomes:

$$\hat{f}(\bar{q}_L, t_L) = \begin{bmatrix} \hat{f}_1 \\ \hat{f}_2 \end{bmatrix} = \begin{bmatrix} \frac{(\hat{L} - \hat{b}_1) \hat{m}_L g}{\hat{L}} \\ \frac{\hat{b}_1 \hat{m}_L g}{\hat{L}} \end{bmatrix} \begin{bmatrix} I_3 \\ I_3 \end{bmatrix} e_3 + t_L \begin{bmatrix} I_3 \\ -I_3 \end{bmatrix} \bar{R}_L e_1. \quad (15)$$

The control (4) is:

$$u_{Ri} = M_{Ai}^{-1} (-B_{Ai} \dot{p}_{Ri} - K_{Ai} p_{Ri}) - f_i + \hat{\pi}_{Ai}.$$

Consider the equilibrium condition:

$$0 = m(q, 0, \hat{\pi}_A). \quad (16)$$

(13) is obtained by substituting the last three lines of (15) into (16) and solving the equilibrium condition for the follower robot. Then, (13) can be substituted into the load translational equilibrium (lines 7, 8, and 9 of (16)) to retrieve (12). (10) results from the first three lines of (16) using (12). Finally, (11) can be obtained using (12) and (13) in the last three lines of (16). Equation (14) is obtained applying the analogous of (43).  $\square$

**Definition 3.** *Given a desired load configuration  $\bar{q}_L = (\bar{p}_L, \bar{R}_L)$ , internal force  $t_L \in \mathbb{R}$ , and forcing input  $\pi_A = \hat{\pi}_A(\bar{q}_L, t_L)$ , we define the set of equilibrium configurations as  $\mathcal{Q}(t_L, \bar{q}_L) = \{q \text{ s.t. conditions of Theorem 2 are satisfied}\}$*

Looking at Theorem 2, we can distinguish between two scenarios:

*Scenario 1:* If  $t_L = 0$ , condition (11) implies that the attitude of the load is such that  $R_L^{eq} e_1$  is aligned to  $e_3$ , and conditions (12) and (13) imply that both cables are vertical. In other words, the load at the equilibrium is, irrespective to the parametric uncertainties, aligned with the vertical direction; even an infinitesimal parametric uncertainty would lead the load to this undesired configuration in which the vertical load is aligned with the two vertical cables. Such a configuration is clearly not realizable. Note that the position error of the system at the equilibrium still depends on the parametric uncertainties (see condition (10)). One can express the alignment between  $R_L^{eq} e_1$  and  $e_3$  as  $(R_L^{eq} e_1)^\top e_3 = \pm 1$ . By convention, let us indicate with  $\mathcal{Q}_1(0, \bar{q}_L)$  the system equilibrium configuration in which  $(R_L^{eq} e_1)^\top e_3 = +1$  holds, namely the one in which the leader robot is above and the follower robot below, and with  $\mathcal{Q}_2(0, \bar{q}_L)$  the other equilibrium configuration. Fig 3a illustrates the aforementioned equilibrium configurations. Note also that there is an additional possibility. With simple manipulation, remembering that  $\hat{b}_1 = b_1 + \Delta b$ ,  $\hat{b}_2 = b_2 + \Delta b_2$ ,

$\hat{L} = L + \Delta_L$ , one can easily find that the term in (11) becomes:

$$\left( b_1 m_L - \frac{\hat{b}_1 \hat{m}_L L}{\hat{L}} \right) = \Delta_m b_1 + \frac{\Delta_{b2}}{\hat{L}} \hat{m}_L b_1 - \frac{\Delta_{b1}}{\hat{L}} \hat{m}_L b_2 := \xi. \quad (17)$$

If  $\xi = 0$ , (11) is verified for every value of  $\mathbf{R}_L$ , and hence the equilibrium configurations  $\mathcal{Q}(0, \bar{\mathbf{q}}_L)$  are infinite and such that the attitude of the load at equilibrium is arbitrary. This happens in the special case in which the parameters of the system are exactly known (this situation is the one we analyzed in [31] and which we can now see as a special case with  $\xi = 0$ ). Indeed,  $\xi = 0$  is verified also if the cable parameters are the sole uncertain ones, as it will be also more deeply discussed in the following. See 3b for a schematic representation of the mentioned equilibrium configurations.

*Scenario 2:* If  $t_L \neq 0$ , condition (11) holds when the vectors  $\mathbf{R}_L^{eq} \mathbf{e}_1$  and

$$(\xi g \mathbf{e}_3 + t_L \bar{\mathbf{R}}_L \mathbf{e}_1) \quad (18)$$

are aligned. Similar to before, this condition holds in two possible cases: when the vectors are aligned and point in the same direction, or when they are aligned but point in opposite directions. Let us indicate with  $\mathbf{R}_L^{eq+}$  the attitude of the load for which condition (11) holds and the two vectors  $\mathbf{R}_L^{eq} \mathbf{e}_1$  and (18) point in the same direction. We indicate the corresponding load equilibrium configuration as  $\mathcal{Q}^+(t_L, \bar{\mathbf{q}}_L)$ . In the other case, when the two aforementioned vectors point in opposite directions, at the equilibrium one has that  $\mathbf{R}_L^{eq-} = \mathbf{R}_L^{eq+} \mathbf{R}_{z_L}(\pi)$ ; we indicate the corresponding equilibrium configuration as  $\mathcal{Q}^-(t_L, \bar{\mathbf{q}}_L)$ . Depending on the sign of  $t_L$  in  $\hat{\pi}_A$ , the forces in the cables place the load under tension in one equilibrium configuration and under compression in the other. Figure 3c represents these equilibrium configurations.

*Remark 2.* Under the hypothesis that  $\bar{\theta} \neq \pi/2 + k\pi$ , with  $k \in \mathbb{N}$ , and  $t_L \neq 0$ , (11) tells us that, at the equilibrium, the following holds:

$$\psi = \bar{\psi} + k\pi \quad (19)$$

$$\theta = \bar{\theta} + \text{atan2}(-\xi g, t_L \cos \bar{\theta}) + k\pi. \quad (20)$$

In other words, *the uncertainties have no effect on the yaw angle at equilibrium*.  $\psi$  may differ from  $\bar{\psi}$  by  $\pi$  because, as already discussed, both  $\mathcal{Q}^+(t_L, \bar{\mathbf{q}}_L)$  and  $\mathcal{Q}^-(t_L, \bar{\mathbf{q}}_L)$  are equilibrium configurations. Moreover, (20) tells us that not only is the attitude error proportional to the amount of uncertainty but also that, as  $t_L$  decreases, the load at the equilibrium becomes *increasingly vertical*. Eventually, for  $t_L = 0$  and there are uncertain parameters ( $\xi \neq 0$ ), (11) leads to  $\mathbf{e}_1 \times \mathbf{R}_L^\top \mathbf{e}_3 = \mathbf{0}$ . Namely, as we have already seen, the load at the equilibrium is aligned with the vertical direction and the two cables are vertical despite the value of  $\xi \neq 0$ . In other words, if  $t_L = 0$  the load attitude error is unaffected by the parametric uncertainties: the load will reach the same, clearly undesired, configuration regardless of the smallest  $\xi \neq 0$ .

In the remainder of this section, we briefly analyze the effects of each uncertain parameter on the final equilibrium.

#### A. Uncertainty on the load mass $m_L$

In this subsection, we only discuss an uncertainty in the load's mass, while the other parameters are regarded as perfectly known. Equations (10)-(13) become:

$$\mathbf{p}_{R1}^{eq} = \hat{\mathbf{p}}_{R1} - \mathbf{K}_{A1}^{-1} \Delta_m g \mathbf{e}_3 \quad (21)$$

$$b_1 \mathbf{S}(\mathbf{e}_1) \mathbf{R}_L^{eq\top} g \Delta_m \mathbf{e}_3 + t_L \mathbf{L} \mathbf{S}(\mathbf{e}_1) \mathbf{R}_L^{eq\top} \bar{\mathbf{R}}_L \mathbf{e}_1 = \mathbf{0} \quad (22)$$

$$\mathbf{f}_1^{eq} = m_L g \mathbf{e}_3 - \frac{b_1 \hat{m}_L g}{L} \mathbf{e}_3 + t_L \bar{\mathbf{R}}_L \mathbf{e}_1 = \hat{\mathbf{f}}_1 + \Delta_m g \mathbf{e}_3 \quad (23)$$

$$\mathbf{f}_2^{eq} = \frac{b_1 \hat{m}_L g}{L} \mathbf{e}_3 - t_L \bar{\mathbf{R}}_L \mathbf{e}_1 = \hat{\mathbf{f}}_2. \quad (24)$$

The position of the load CoM at the equilibrium is different from  $\bar{\mathbf{p}}_L$  and can be computed from (14) using (21)-(23).

It is worth noting that the leader robot can detect a mismatch between the known commanded  $\hat{\mathbf{f}}_1$  and the actual force  $\mathbf{f}_1^{eq}$  measured at steady state. Such a discrepancy solely depends on  $\Delta_m$ , according to (23). Thus, the leader robot can compute  $\Delta_m$  and, knowing the nominal value  $\hat{m}_L$ , retrieve the actual value of the load mass,  $m_L$ , which it can use to adjust its own reference force and position. However, in order for both robots to know the proper parameter value, a one-time data exchange between them might be established to pass knowledge of  $m_L$  from the leader to the follower. At that point, the robots would be in a situation in which there is no uncertainty on the system parameters. Thus, [31] shows that, given  $t_L \neq 0$ , the robots could stabilize the load at the desired equilibrium. However, this interesting remark falls out of the scope of this paper that focuses on a communication-less approach.

#### B. Uncertainty on the load length, $L$ , or CoM position, $b_1$

Uncertainties on one of these two parameters have similar effects. In one case,  $\hat{b}_1 \neq b_1$ , namely the load CoM is aligned to the cables attachment points on the load at an uncertain position but  $L$  is exactly known; in the other case,  $b_1$  is exactly known but  $L$  is not. In both cases, at the equilibrium, the following conditions hold:

$$\mathbf{p}_R^{eq} \mathbf{1} = \hat{\mathbf{p}}_{R1} \quad (25)$$

$$\mathbf{S}(\mathbf{e}_1) \mathbf{R}_L^{eq\top} (t_L \bar{\mathbf{R}}_L \mathbf{e}_1 + y m_L g \mathbf{e}_3) = \mathbf{0} \quad (26)$$

$$\mathbf{f}_1^{eq} = \hat{\mathbf{f}}_1 \quad (27)$$

$$\mathbf{f}_2^{eq} = \hat{\mathbf{f}}_2, \quad (28)$$

where  $y = \Delta_b$  in one case, and  $y = b_1 L \Delta_\ell$  in the other;  $\hat{\mathbf{p}}_{R1}$ ,  $\hat{\mathbf{f}}_1$ , and  $\hat{\mathbf{f}}_2$  are computed from (8) and (9), where the corresponding uncertain parameter is used in place of the real one.

In this case, the leader robot position and both cable forces at the equilibrium coincide with the respective reference values available to the robots (see (25)-(28)). Consequently, *it is not possible for any of the robots to estimate the uncertain parameter at the equilibrium based on the local information they possess*.

### C. Uncertainty on the cable length $l_{0i}$ or stiffness $k_i$

Consider an uncertainty on the parameters of the  $i$ -th cable such that the rest length is  $l_{0i} \neq \hat{l}_{0i}$  and the stiffness is  $k_i \neq \hat{k}_i$ . At the equilibrium, it holds that  $\mathbf{f}_i^{eq} = \bar{\mathbf{f}}_i$ ,

$$\mathbf{R}_L^{eq} = \bar{\mathbf{R}}_L. \quad (29)$$

$$\mathbf{p}_{R1}^{eq} = \hat{\mathbf{p}}_{R1} = \bar{\mathbf{p}}_L + \bar{\mathbf{R}}_L^L \mathbf{b}_1 + \left( \frac{\|\bar{\mathbf{f}}_1\|}{\hat{k}_1} + \hat{l}_{01} \right) \frac{\bar{\mathbf{f}}_1}{\|\bar{\mathbf{f}}_1\|}, \quad (30)$$

and the value of  $\mathbf{p}_L$  at the equilibrium is:

$$\mathbf{p}_L^{eq} = \hat{\mathbf{p}}_{R1} - \bar{\mathbf{R}}_L^L \mathbf{b}_1 - \left( \frac{\|\bar{\mathbf{f}}_1\|}{k_1} + l_{01} \right) \frac{\bar{\mathbf{f}}_1}{\|\bar{\mathbf{f}}_1\|} \quad (31)$$

We highlight that knowledge about the cable properties is required only when computing the reference position of the leader robot, according to (8). What is more, only the information about  $k_1$  and  $l_{01}$  is required. We conclude that knowledge of  $l_{02}$  and  $k_2$ , is not necessary to stabilize the load at a desired pose. Moreover,  $l_{01}$  and  $k_1$  have no effect on the load attitude at equilibrium but they do influence the load position. This can be easily seen by substituting (30) into (31) with  $l_{01} \neq \hat{l}_{01}$  and  $k_1 \neq \hat{k}_1$ . Note that, since the robots' forces and the leader robot's position at the equilibrium coincide with the reference values available to the robots themselves, they are not aware of the load pose error induced by this uncertainty.

## IV. STABILITY ANALYSIS

In this section, we shall analyze the stability of the equilibrium configurations discovered in Sec III. First, being  $\mathbf{x} = (\mathbf{q}, \mathbf{v})$  the state of the system, we define the following equilibrium states (subspaces of the state space):

- $\mathcal{X}(0, \bar{\mathbf{q}}_L) = \{\mathbf{x} : \mathbf{q} \in \mathcal{Q}(0, \bar{\mathbf{q}}_L), \mathbf{v} = \mathbf{0}\},$
- $\mathcal{X}_1(0, \bar{\mathbf{q}}_L) = \{\mathbf{x} : \mathbf{q} \in \mathcal{Q}_1(0, \bar{\mathbf{q}}_L), \mathbf{v} = \mathbf{0}\},$
- $\mathcal{X}_2(0, \bar{\mathbf{q}}_L) = \{\mathbf{x} : \mathbf{q} \in \mathcal{Q}_2(0, \bar{\mathbf{q}}_L), \mathbf{v} = \mathbf{0}\},$
- $\mathcal{X}^+(t_L, \bar{\mathbf{q}}_L) = \{\mathbf{x} : \mathbf{q} \in \mathcal{Q}^+(t_L, \bar{\mathbf{q}}_L), \mathbf{v} = \mathbf{0}\},$
- $\mathcal{X}^-(t_L, \bar{\mathbf{q}}_L) = \{\mathbf{x} : \mathbf{q} \in \mathcal{Q}^-(t_L, \bar{\mathbf{q}}_L), \mathbf{v} = \mathbf{0}\}.$

**Theorem 3.** *Let us consider a desired load configuration  $\bar{\mathbf{q}}_L$ . For the system (5), let the constant forcing input be  $\hat{\pi}_A$ . Then,*

- $\mathcal{X}_1(0, \bar{\mathbf{q}}_L)$  is asymptotically stable if  $\xi > 0$  and unstable if  $\xi < 0$ ;
- $\mathcal{X}_2(0, \bar{\mathbf{q}}_L)$  is asymptotically stable if  $\xi < 0$  and unstable if  $\xi > 0$ .
- $\mathcal{X}(0, \bar{\mathbf{q}}_L)$  is a set of marginally stable equilibrium points if  $\xi = 0$ .
- $\mathcal{X}^+(t_L, \bar{\mathbf{q}}_L)$  is asymptotically stable
- $\mathcal{X}^-(t_L, \bar{\mathbf{q}}_L)$  is unstable.

*Proof.* Consider the following Lyapunov candidate function:

$$\begin{aligned} V(\mathbf{x}) = & \frac{1}{2} (\mathbf{v}_R^\top \mathbf{M}_A \mathbf{v}_R + \mathbf{e}_R^\top \mathbf{K}_A \mathbf{e}_R + \mathbf{v}_L^\top \mathbf{M}_L \mathbf{v}_L + \\ & + k_1 (\|\mathbf{l}_1\| - l_{01})^2 + k_2 (\|\mathbf{l}_2\| - l_{02})^2) - \mathbf{l}_1^\top \mathbf{f}_1^{eq} + \\ & - \mathbf{l}_2^\top \mathbf{f}_2^{eq} + V_0 + V_R(\mathbf{x}), \end{aligned} \quad (32)$$

where the robot position error is  $\mathbf{e}_R = \mathbf{p}_R - \mathbf{p}_R^{eq}$ ,  $V_0$  is constant, and  $V_R(\mathbf{x})$  is an additional term explained in the following. Function (32) is composed of standard positive definite

quadratic terms equal to zero in the equilibrium points and by two terms of the form  $\frac{1}{2} k_i (\|\mathbf{l}_i\| - l_{0i})^2 - \mathbf{l}_i^\top \mathbf{f}_i^{eq}$ , call them  $V_i(\mathbf{x})$ : these are linked to the elastic energy of the cables and have a minimum at the equilibrium as well. A detailed proof of the former point can be found in [31]. The proof first shows that  $V_i(\mathbf{x})$  is *radially unbounded*, i.e.,  $\lim_{\|\mathbf{x}\| \rightarrow \infty} V_i(\mathbf{x}) = \infty$ . Then, based on this result and Theorem 1.15 of [39], the term has a global minimum. Finally, it has been shown that the global minimum of  $V_i(\mathbf{x})$  corresponds to the considered equilibrium [31].

We define the value of  $V_i(\mathbf{x})$  at the equilibrium (its minimum value) as  $-V_0$ , and we cancel it in (32) so that its value at the equilibrium is zero.

Let us start considering  $\mathcal{X}_1(0, \bar{\mathbf{q}}_L)$  and  $\xi > 0$ . In this case, we set  $V_R(\mathbf{x}) = \xi g(1 - \mathbf{e}_3^\top \mathbf{R}_L \mathbf{e}_1)$ . With this choice, (32) is zero in  $\mathcal{X}_1(0, \bar{\mathbf{q}}_L)$  because also the term  $1 - \mathbf{e}_3^\top \mathbf{R}_L \mathbf{e}_1$  is zero in  $\mathcal{X}_1(0, \bar{\mathbf{q}}_L)$  by definition (load aligned with the vertical with  $\mathbf{R}_L \mathbf{e}_1$  and  $\mathbf{e}_3$  pointing in the same direction) and positive elsewhere (the scalar product  $\mathbf{e}_3^\top \mathbf{R}_L \mathbf{e}_1 \leq 1$  because  $\mathbf{e}_3$  and  $\mathbf{R}_L \mathbf{e}_1$  have both unit norm).

Studying the sign of the time derivative of (32), using (5), (2), and (9), we obtain  $\dot{V}(\mathbf{x}) = -\mathbf{v}_R^\top \mathbf{B}_A \mathbf{v}_R - \omega_L^\top \mathbf{B}_L \omega_L$ , which is clearly negative semidefinite. In particular, let us define  $\mathcal{E} = \{\mathbf{x} : \dot{V}(\mathbf{x}) = 0\}$ . In this case, we have  $\mathcal{E} = \{\mathbf{x} : \mathbf{v}_R = \mathbf{0}, \omega_L = \mathbf{0}\}$ .

Since  $\dot{V}$  is only negative semidefinite, we rely on *LaSalle's invariance principle* to complete the proof: one can easily verify from (5) that the largest invariant set in  $\mathcal{E}$  is  $\mathcal{X}_1(0, \bar{\mathbf{q}}_L)$ .

Analogous reasoning can be used when  $\xi < 0$ . The computation of  $\dot{V}$  does not change, and it is, thus, negative semidefinite. However,  $\mathcal{X}_1(0, \bar{\mathbf{q}}_L)$  is a set of accumulation for the points where  $V(\mathbf{x}) < 0$  if  $\xi < 0$ . To see this, consider  $\mathbf{v} = \mathbf{0}$  and all quantities at the equilibrium apart from  $\mathbf{R}_L$ , which is such that  $\mathbf{e}_3^\top \mathbf{R}_L \mathbf{e}_1 = 1 - \varepsilon$ , with  $\varepsilon > 0$  arbitrarily small, meaning that  $\mathbf{R}_L$  is arbitrarily close to  $\mathbf{R}_L^{eq}$ . Under this conditions, we have that  $V(\mathbf{x}) = g\xi\varepsilon < 0$ . All conditions of *Chetaev's theorem* (the formulation of both this and La Salle's invariance principle can be found, e.g., in [40]) are satisfied, and we can conclude that  $\mathcal{X}^+(t_L, \bar{\mathbf{q}}_L)$  is unstable.

To show that  $\mathcal{X}_2(0, \bar{\mathbf{q}}_L)$  is asymptotically stable if  $\xi < 0$ , we set  $V_R(\mathbf{x}) = -\xi g(1 + \mathbf{e}_3^\top \mathbf{R}_L \mathbf{e}_1)$ , which is zero in  $\mathcal{X}_2(0, \bar{\mathbf{q}}_L)$  (when  $\mathbf{e}_3^\top \mathbf{R}_L \mathbf{e}_1 = -1$  by definition), and positive elsewhere. The same Lyapunov candidate function is used to show that  $\mathcal{X}_2(0, \bar{\mathbf{q}}_L)$  is unstable if  $\xi > 0$ . The reasoning is exactly dual to the previous case, so it is here omitted for the sake of space.

Consider now  $\xi = 0$ . We set  $V_R(\mathbf{x}) = 0$ , so that (32) is zero in  $\mathcal{X}(0, \bar{\mathbf{q}}_L)$  and positive elsewhere. Moreover,  $\dot{V}$  is as before, hence negative semidefinite. One easily shows that the largest invariant set is  $\mathcal{X}(0, \bar{\mathbf{q}}_L)$ . We can thus say that the system state converges to a state  $\mathbf{x} \in \mathcal{X}(0, \bar{\mathbf{q}}_L)$ , which is, however, composed of a continuum of equilibrium points, hence they are only *marginally stable*.

Finally, we study the stability of the equilibrium points when  $t_L \neq 0$ . In this case, we set  $V_R(\mathbf{x}) = -(\xi g \mathbf{e}_3 + t_L L \bar{\mathbf{R}}_L \mathbf{e}_1)^\top \mathbf{R}_L \mathbf{e}_1 + V_0'$ , with  $V_0' = (\xi g \mathbf{e}_3 + t_L L \bar{\mathbf{R}}_L \mathbf{e}_1)^\top \mathbf{R}_L^{eq} \mathbf{e}_1$ . Clearly,  $V_R(\mathbf{x})$  and hence  $V(\mathbf{x})$  are zero at the equilibrium. Moreover,  $V_R(\mathbf{x})$  is positive elsewhere by definition of  $\mathcal{X}^+(t_L, \bar{\mathbf{q}}_L)$  ( $\xi g \mathbf{e}_3 + t_L L \bar{\mathbf{R}}_L \mathbf{e}_1$



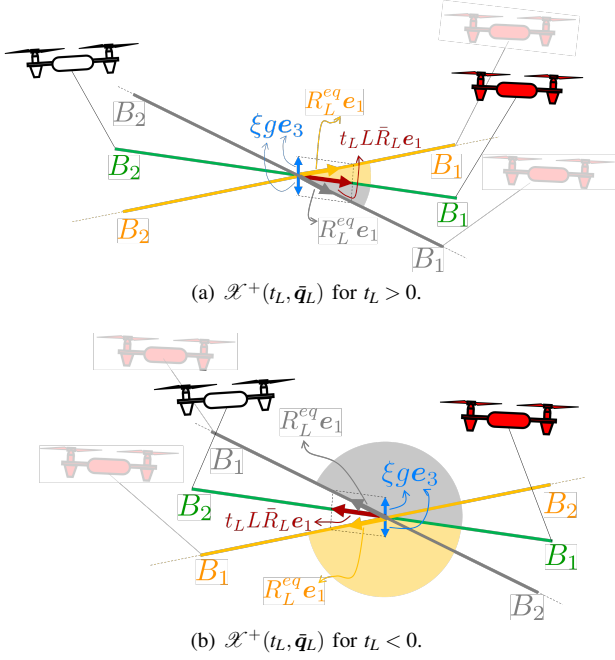


Fig. 4: Attitude of the load in the asymptotically stable equilibrium points  $\mathcal{X}^+(t_L, \bar{q}_L)$  when  $t_L \neq 0$ . In the two plots, the green configuration is the desired one, described by vector  $\bar{R}_L e_1$ , the grey and yellow beams correspond to the equilibrium when  $\xi > 0$  (blue vector  $\xi g e_3$  pointing upwards) and  $\xi < 0$ , respectively. For  $t_L > 0$  (on top), the displacement between  $\bar{R}_L e_1$  and  $R_L^{\text{eq}} e_1$  is smaller than in the case in which  $t_L < 0$  (below). Circular sectors highlight the displacement between the desired and the actual equilibrium attitude of the load. Also, the leader robots in the equilibrium configurations are shown in transparency to better convey the difference between the top and bottom situations.

and  $R_L e_1$  are aligned and point in the same direction when  $R_L = R_L^{\text{eq}}$ , so that  $V_R(x)$  has its minimum in  $\mathcal{X}^+(t_L, \bar{q}_L)$ . Moreover,  $\dot{V}(x) = -v_R^\top B_A v_R - \omega_L^\top B_L \omega_L$ , and the application of LaSalle's invariance principle similar to before leads to the conclusion that  $\mathcal{X}^+(t_L, \bar{q}_L)$  is an asymptotically stable equilibrium point. To show the instability of  $\mathcal{X}^-(t_L, \bar{q}_L)$ , we use the same choice for  $V_R(x)$ . However, since  $\xi g e_3 + t_L L \bar{R}_L e_1$  and  $R_L e_1$  are anti-parallel in  $\mathcal{X}^-(t_L, \bar{q}_L)$ ,  $V_R(x)$  is still zero at the equilibrium but negative when  $R_L$  is arbitrarily close to  $R_L^{\text{eq}}$ .  $\mathcal{X}^-(t_L, \bar{q}_L)$  is a point of accumulation for the points in which  $\dot{V}(x)$  is negative, while  $\dot{V}(x)$  remains negative semi-definite. For Chetaev's theorem, we conclude that  $\mathcal{X}^-(t_L, \bar{q}_L)$  is unstable.  $\square$

It is important to highlight that, as shown in Figure 4, for  $t_L > 0$ ,  $\mathcal{X}^+(t_L, \bar{q}_L)$  corresponds to a configuration of the system in which  $R_L^{\text{eq}}$  (irrespective of the sign of  $\xi$ ) is the closest to  $\bar{R}_L$ , namely to the desired attitude, with a displacement due to the parametric uncertainty. Instead, for  $t_L < 0$ , is  $\mathcal{X}^-(t_L, \bar{q}_L)$  the equilibrium point in which the configuration of the load is the closest to the desired one. We can say that these configurations are the most desirable equilibrium configuration of the load in the presence of parametric uncertainties. *Theorem 3* tells us that  $t_L > 0$  stabilizes the most desirable equilibrium configuration of the load, which is, instead, unstable if  $t_L < 0$ .

## V. THE ROLE OF THE INTERNAL FORCES ON THE LOAD ERROR CAUSED BY PARAMETRIC UNCERTAINTIES

In this section, we provide a formal analysis of the role that the internal force plays in determining the load pose at the equilibrium in the presence of parametric uncertainties. We shall consider the simultaneous presence of all the uncertainties listed in Sec III. We start considering the load *attitude*.

### A. Load attitude error

**Theorem 4.** Let us define the load attitude error at the equilibrium point  $\mathcal{X}^+(t_L, \bar{q}_L)$  as:

$$e_{R_L} = \|R_L^{\text{eq}} e_1 \times \bar{R}_L e_1\|^2. \quad (33)$$

$e_{R_L}$  is inversely proportional to the intensity of the internal force,  $t_L$ . Furthermore, the error sensitivity w.r.t  $\Delta_m$ ,  $\Delta_b$ ,  $\Delta_{k_i}$ ,  $\Delta_{l_{0i}}$ , and  $\Delta_\ell$ , defined as  $\frac{\partial e_{R_L}}{\partial \Delta_m}$ ,  $\frac{\partial e_{R_L}}{\partial \Delta_b}$ ,  $\frac{\partial e_{R_L}}{\partial \Delta_{k_i}}$ ,  $\frac{\partial e_{R_L}}{\partial \Delta_{l_{0i}}}$ , and  $\frac{\partial e_{R_L}}{\partial \Delta_\ell}$ , respectively, is given by:

$$\frac{\partial e_{R_L}}{\partial \Delta_m} = \frac{-2\hat{b}_1 \hat{\ell} g^2 \alpha \cos \theta^2}{t_L^2 L^2} \quad (34)$$

$$\frac{\partial e_{R_L}}{\partial \Delta_b} = \frac{-2\hat{m}_L \hat{\ell} g^2 \alpha \cos \theta^2}{t_L^2 L^2} \quad (35)$$

$$\frac{\partial e_{R_L}}{\partial \Delta_{k_i}} = \frac{\partial e_{R_L}}{\partial \Delta_{l_{0i}}} = 0 \quad (36)$$

$$\frac{\partial e_{R_L}}{\partial \Delta_\ell} = \frac{-2\hat{b}_1 \hat{m}_L g^2 \alpha \cos \theta^2}{t_L^2 L^2} \quad (37)$$

where

$$\alpha := (b_1 - \Delta b)(m_L - \Delta m)(\ell - \Delta_\ell) - m_L b_1.$$

*Proof.* Rewrite (11) in  $\mathcal{F}_W$  as:

$$R_L^{\text{eq}} e_1 \times \left[ \left( b_1 m_L - \frac{\hat{b}_1 \hat{m}_L L}{\hat{L}} \right) g e_3 + t_L L \bar{R}_L e_1 \right] = 0. \quad (38)$$

Define also:

$$\frac{\hat{b}_1 \hat{m}_L L - b_1 m_L \hat{L}}{t_L L \hat{L}} (R_L^{\text{eq}} e_1 \times g e_3) := x. \quad (39)$$

Thus, from (38), we have that  $R_L^{\text{eq}} e_1 \times \bar{R}_L e_1 = x$  and, from (33), that  $e_{R_L} = x^\top x$ . From these it is clear that  $e_{R_L}$  is inversely proportional to  $t_L$ . Regarding the sensitivity, we show the proof for (34) only, because the other cases follow the exactly same analysis. We can write the sensitivity as:

$$\begin{aligned} \frac{\partial e_{R_L}}{\partial \Delta_m} &= 2x^\top \frac{\partial x}{\partial \Delta_m} = \\ &= 2 \left[ \frac{1}{t_L L} R_L^{\text{eq}} e_1 \times (\alpha) g e_3 \right]^\top \left[ \frac{1}{t_L L} R_L^{\text{eq}} e_1 \times (\Delta b - b_1) g e_3 \right] \end{aligned} \quad (40)$$

Eventually, (40) can be rewritten as (34) by remembering that, given three vectors  $a, b$ , and  $c$

$$(a \times b)^\top (a \times c) = |a|^2 (b^\top c) - (a^\top b)(a^\top c).$$

Note that we are considering  $t_L \neq 0$  by assumption.  $\square$

*Remark 3.* The definition in (33) is a suitable metric for the attitude error. Firstly,  $R_L e_1$  is enough to describe the entire



attitude of the *beam-like* load. Secondly,  $e_{R_L}$  is zero when  $\mathbf{R}_L^{eq} = \bar{\mathbf{R}}_L$  and increases with the displacement between the two vectors  $\mathbf{R}_L^{eq} \mathbf{e}_1$  and  $\bar{\mathbf{R}}_L \mathbf{e}_1$ , at least locally (for displacements smaller than  $\pm\pi/2$ ).

Theorem 4 shows that *increasing the intensity of the internal force  $t_L$  not only makes the attitude error smaller in presence of parametric uncertainties, but it also makes the error more robust to variations of such uncertainties.*

This last aspect may be of particular practical interest: as a matter of fact, parametric uncertainty variations take place every time the actual physical parameters of the system change. A possible real-world scenario is the transportation of objects that are slightly different from each other, e.g., in mass and length. One may want to transport the objects without changing every time the controller parameters for the sake of time, thus dealing with varying parametric uncertainties. Especially interesting, as also highlighted in [41], is the variation affecting the center of mass position, which may change online when transporting moving masses, i.e. containers of liquids, or boxes with smaller objects free to move inside. The previous analysis suggests that in all these cases having a larger value of  $t_L$  is of uttermost benefit, resulting in an error less sensitive to the aforementioned parametric variations.

### B. Load position error

Differently from what happens to the load attitude error, the load position error at the equilibrium does not necessarily decrease when  $t_L$  increases. While to claim a positive statement a comprehensive proof is needed as we did in Sec V-A, to deny a positive statement, as we are doing in this section, a counterexample is enough. First, it is easy to see that, when only  $l_{01}$  is uncertain, the load position error at the equilibrium,  $e_{p_L} := \mathbf{p}_L^{eq} - \bar{\mathbf{p}}_L$  is

$$e_{p_L} = \Delta_l \frac{b_2 m g \mathbf{e}_3 + t_L \bar{\mathbf{R}}_L \mathbf{e}_1}{\|b_2 m g \mathbf{e}_3 + t_L \bar{\mathbf{R}}_L \mathbf{e}_1\|}. \quad (41)$$

Eq. (41) tells us that  $e_{p_L}$  is equal to a unit vector multiplied by  $\Delta_{l_{01}}$ , thus, its module is independent of the value of  $t_L$ . Moreover, in the next section, we provide two numerical examples showing that, depending on the specific combination and values of uncertainties,  $e_{p_L}$  may even have a non-monotonic evolution for increasing values of  $t_L$ , with an initial increasing or decay.

However, we show in the following that, preserving the leader-follower architecture and the absence of direct communication between the robots, it is possible to correct the load position error at the equilibrium, ideally bringing it to zero.

We recall that, due to parametric uncertainties, the reference position given to the leader robot is

$$\hat{\mathbf{p}}_{R1} = \bar{\mathbf{p}}_L + \bar{\mathbf{R}}_L^L \hat{\mathbf{b}}_1 + \left( \frac{\|\hat{\mathbf{f}}_1\|}{\hat{k}_1} + \hat{l}_{01} \right) \frac{\hat{\mathbf{f}}_1}{\|\hat{\mathbf{f}}_1\|}. \quad (42)$$

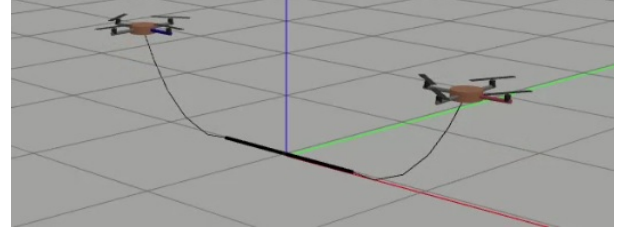


Fig. 5: The robots are taking off in the simulated scenario. The sagging effect reproduced by the cable model employed in the simulator is clearly visible.

By using kinematics, (10), and (42), the load position at the equilibrium is

$$\begin{aligned} \mathbf{p}_L^{eq} &= \mathbf{p}_{R1}^{eq} - \left( \frac{\|\mathbf{f}_1^{eq}\|}{k_1} + l_{01} \right) \frac{\mathbf{f}_1^{eq}}{\|\mathbf{f}_1^{eq}\|} - \mathbf{R}_L^{eq} \mathbf{b}_1 \\ &= \bar{\mathbf{p}}_L + \bar{\mathbf{R}}_L^L \hat{\mathbf{b}}_1 + \left( \frac{\|\hat{\mathbf{f}}_1\|}{\hat{k}_1} + \hat{l}_{01} \right) \frac{\hat{\mathbf{f}}_1}{\|\hat{\mathbf{f}}_1\|} - \mathbf{K}_A^{-1} \Delta_m g \mathbf{e}_3 + \\ &\quad - \left( \frac{\|\mathbf{f}_1^{eq}\|}{k_1} + l_{01} \right) \frac{\mathbf{f}_1^{eq}}{\|\mathbf{f}_1^{eq}\|} - \mathbf{R}_L^{eq} \mathbf{b}_1. \end{aligned} \quad (43)$$

From (43), we have an expression for  $e_{p_L}$ . Now, if the leader robot knows the load position, it can recognize that, at steady state,  $\tilde{\mathbf{p}}_L \neq 0$  holds, and it can adjust its position reference to  ${}^2\hat{\mathbf{p}}_{R1}$  accordingly, with

$${}^2\hat{\mathbf{p}}_{R1} = \hat{\mathbf{p}}_{R1} - e_{p_L}. \quad (44)$$

In this way, there will be a new equilibrium in which the leader robot position is:

$$\mathbf{p}_{R1}^{eq} = {}^2\hat{\mathbf{p}}_{R1} - \mathbf{K}_A^{-1} \Delta_m g \mathbf{e}_3 \quad (45)$$

and thus (43) becomes:

$$\mathbf{p}_L^{eq} = \bar{\mathbf{p}}_L \quad (46)$$

It is important to highlight that the leader robot position only influences the load position and not the attitude at the equilibrium, which depends only upon the reference forces computed based on  $\bar{\mathbf{R}}_L$ . Indeed, by evaluating (5) at the equilibrium, the last three rows are:

$$\mathbf{S}({}^L\mathbf{b}_1) \mathbf{R}_L^{eq\top} \mathbf{f}_1^{eq} + \mathbf{S}({}^L\mathbf{b}_2) \mathbf{R}_L^{eq\top} \mathbf{f}_2^{eq} = \mathbf{0},$$

which become, substituting  $\mathbf{f}_i^{eq}$ , eq. (11). Hence, the leader robot can correct the position error of the load, while the internal force independently acts decreasing the attitude error. Because the load's the position can be steered relying solely on the leader robot, unlike the load's attitude, which is determined by the cooperative actions of both robots, the control approach can maintain its distributed nature. However, to correct the load position error, the leader robot must have access to the load position. This implies that additional sensors would be required on the leader robot side, e.g., a camera, to accomplish this task.

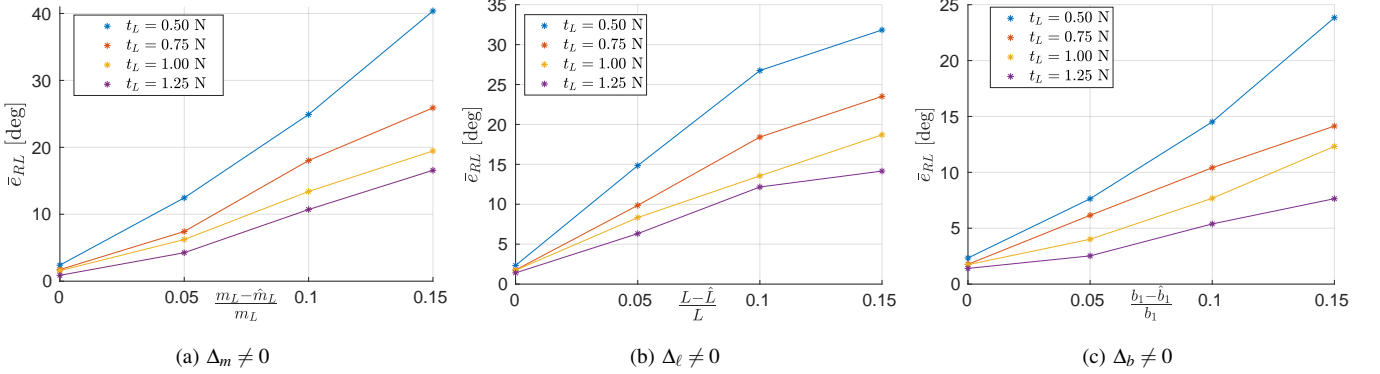


Fig. 6: Each point in the plots is a value of the average attitude error at steady state in a simulation with  $t_L$  as indicated in the legend, and parametric uncertainty as indicated in the x-axis of the corresponding plot. A total of 40 simulation results are known in these plots.

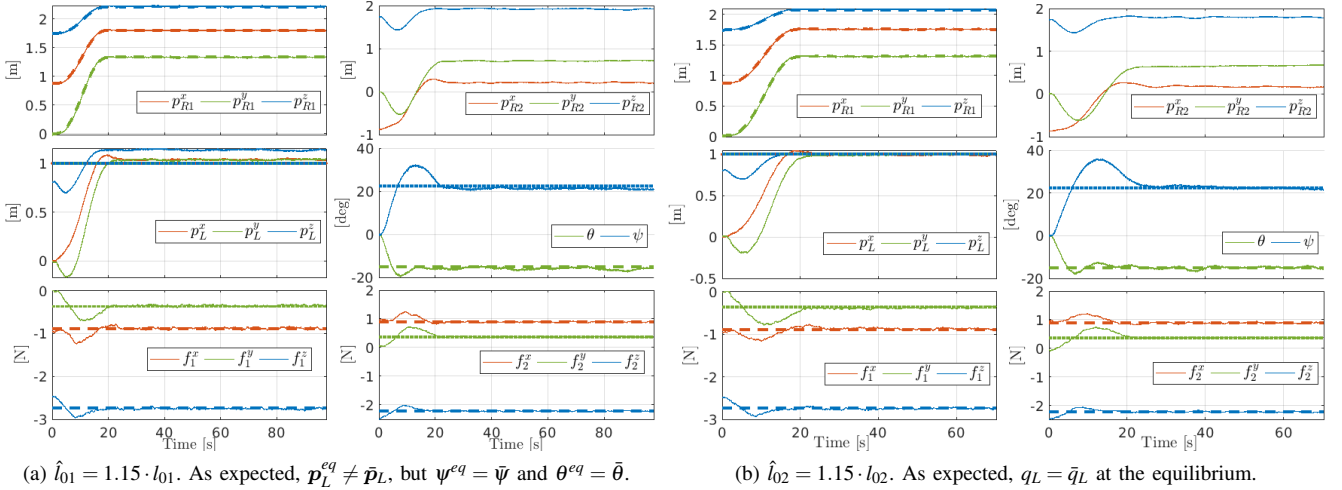


Fig. 7: Simulations for cable parameter uncertainties and  $t_L = 1\text{N}$ . Dotted lines of the same color indicate the corresponding desired quantities.

## VI. NUMERICAL VALIDATION

Extensive numerical experiments have been carried out using an URDF description of the system and ODE physics engine in Gazebo. We avoided validating the theoretical results on the same equations used to derive them. The main differences between the control model used to derive a fully satisfactory theoretical analysis and the complex simulation model used to study the applicability of the theoretical results in the real world are in the following.

- Under-actuated quadrotors have been deliberately preferred for the validation since they represent the worst-case in terms of the validity of some of the assumptions made in the theoretical analyses. Validation using fully-actuated aerial robots would have seemed, instead, limiting.
- The cables are subject to sagging, which is obtained by using a series of several links interconnected by passive universal joints, as can be seen in Fig. 5.
- In the validation, there is no guarantee of perfect trajectory tracking as assumed in the theory but a standard position controller [42] is implemented for each robot.

- The wrench observer proposed in [43] is used to estimate the force applied by the cable on the robot. The observer introduces noisy and delayed measurements when compared to ideal force measurement.

The control software has been implemented in Matlab-Simulink using the GGenerator of Modules GenoM<sup>4</sup>. The interface between Matlab and Gazebo is also managed by a Gazebo-genom3 plugins<sup>5</sup>. All phases of a physical experiment, starting with takeoff, are replicated in the simulated environment using a state machine, ensuring that the results are as realistic as possible. After the takeoff, the two robots lift the load, and the admittance controller is activated right after.

The robot models are two quadrotors weighting 1.03 kg and having a maximum thrust for each propeller of 6 N. They are equipped with two light cables of length 1 m and attached to a bar. The bar is a one-meter-long link with a mass of 0.5 kg.

1) *Case of  $t_L > 0$ :* Fig. 6 contains the average load attitude error at a steady state in a total of 40 simulations. The average is computed in a 2-second time window. In all

<sup>4</sup><https://git.openrobots.org/projects/genom3>

<sup>5</sup><https://git.openrobots.org/projects/mrsim-gazebo>

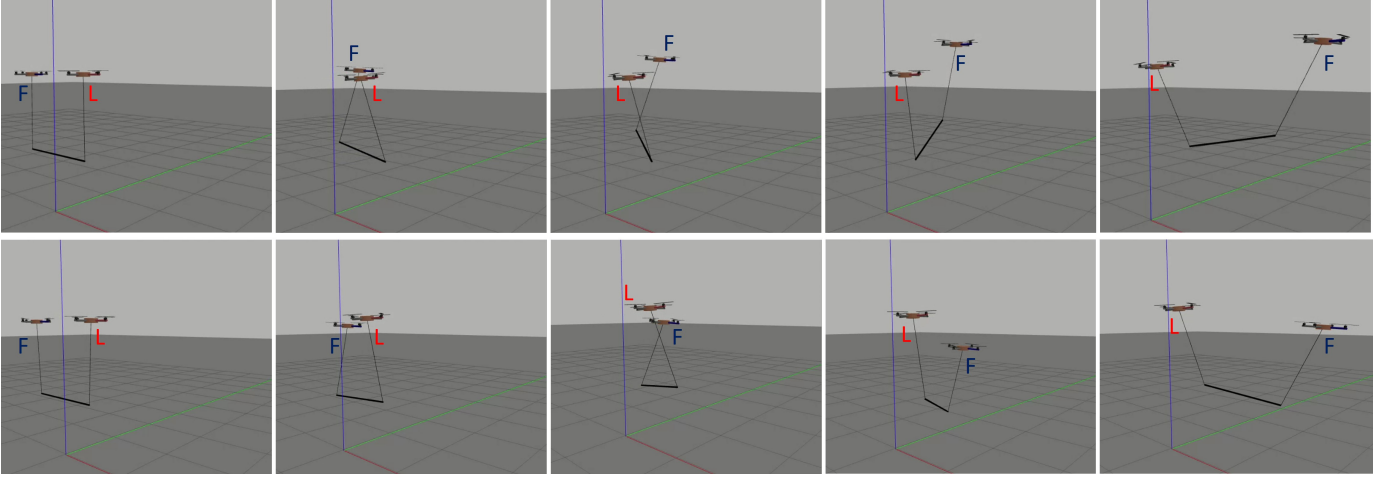


Fig. 8: Frames from two simulated scenarios for  $t_L < 0$ . Top:  $\xi < 0$ ; bottom:  $\xi > 0$ . The leader has a red arm and the follower a blue arm. However, to facilitate the distinction among them, a red letter ‘L’ indicated the leader and a blue ‘F’ the follower.

those simulations,  $\bar{\mathbf{p}}_L = [1 \ 1 \ 1]^\top$  m, the load desired yaw is  $\bar{\psi} = \frac{\pi}{8}$  radians, and the desired pitch  $\bar{\theta} = -\frac{\pi}{12}$  radians. In each of the three plots in Fig. 6, for four different values of the internal force,  $t_L = \{0.5, 0.75, 1, 1.25\}$  N, four different simulation results are displayed for each relative error equal to 0%, 5%, 10%, 15% on a specific uncertain parameter considered separately from the others. Specifically, Fig. 6a, considers the uncertainty on  $m_L$ , Fig. 6b on  $L$ , and Fig. 6c on  $b_1$ . Even in the absence of uncertainties, small errors of less than 2.5 degrees in the bar’s attitude control can be found. This can be due to minor tracking errors or possible biases in the wrench observer, which estimations are unbiased as soon as the robot takes off. These considerations ignore the external forces applied by the loose cables at the startup phase. From all the three figures one can appreciate the beneficial effect of larger values of  $t_L$  on the attitude error: for the same value of the uncertainty, the attitude error decreases if the  $t_L$  increases. Moreover, the plots show that for every value of  $t_L$ , increasing the uncertainty on one parameter increases the attitude error, as expected, but, especially, the increase is smaller for high values of  $t_L$  (this can be seen by the slope of the lines in the plots). These results confirm the theoretical findings collected in Theorem 4. Fig. 7a and 7b provide validation of the theoretical results on the effect of the uncertainties affecting the cable parameters. The leader robot position reference is not given as a step, but the robot follows a 5-th order polynomial trajectory to reach the desired position. An error of 15% is considered to affect the length of the leader and follower robot’s cable in Fig. 7a and 7b, respectively. In both cases,  $t_L = 1$  N. Note that the displayed time starts after the admittance controller activation. The reader can appreciate how uncertainties on the leader robot’s cable model only cause  $\mathbf{p}_L^{eq} \neq \bar{\mathbf{p}}_L$ , while  $\mathbf{R}_L^{eq} = \bar{\mathbf{R}}_L$ , and how the follower robot’s cable parameters are not needed to control the load pose, as expected from (31) and (29).

2) *Case of  $t_L < 0$ :* Here we show the behavior of the system with  $t_L < 0$ . The unstable nature of the desired configuration with no parametric uncertainties was shown in [31]. The simulations of the realistic system, in accordance with Theorem

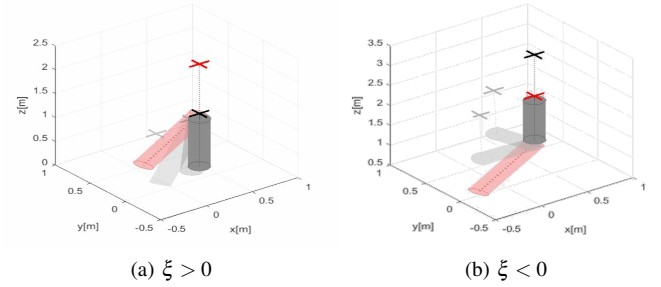


Fig. 9: Superposition of different instants of simulations with  $\xi \neq 0$  and  $t_L = 0$ . The solid image is the final equilibrium. The grey cylinder is the load, and the red cross is the leader robot. The red cylinder is the desired (identical to the initial) pose of the load.

3, show that the new equilibrium is still unstable when the parametric uncertainties are considered. We report the results of two simulations with  $\bar{\mathbf{p}}_{R1} = [0 \ 0 \ 1]^\top$  m,  $\bar{\psi} = \frac{\pi}{8}$  radians, and  $\bar{\theta} = 0$  radians (desired horizontal bar). We simulate an uncertainty of 5% both on  $m_L$  and  $L$  such that (i)  $\xi > 0$  (we chose  $\hat{m}_L < m_L$  and  $\hat{L} > L$ ) and (ii)  $\xi < 0$  (thanks to  $\hat{m}_L > m_L$  and  $\hat{L} < L$ ). In both cases, we obtained that, at steady state,  $\psi = \bar{\psi} - \pi$ , while  $\theta$  varies according to the sign of  $\xi$ , as expected (see Fig. 4b). The cable forces were observed to be as desired, except for the vertical component of  $\mathbf{f}_1$ , as expected due to  $\Delta_m \neq 0$  according to (23). Fig. 8 shows the behavior of the system in the described cases through screenshots of the Gazebo environment.

3) *Case of  $t_L = 0$ :* When it comes to the case in which  $\xi \neq 0$  and  $t_L = 0$ , clearly, the sole equilibrium configurations are not really attainable: all elements of the system are supposed to be aligned vertically, one on top of the others (see Figure 3a). When simulating such condition in Gazebo, we found that numerical issues arise as the system approaches the expected configuration in which the link that models the load and those that model the cables are vertically aligned. Despite the practical irrelevance of the considered case, with the objective of demonstrating the validity of the theoretical

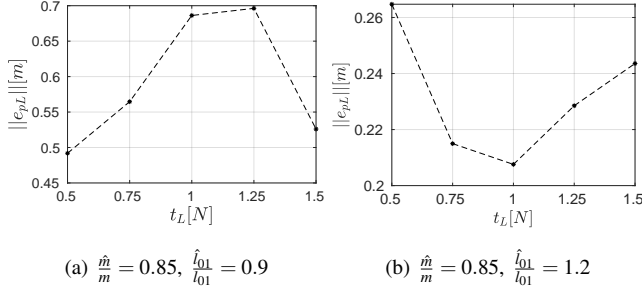


Fig. 10:  $\|e_{pL}\|$  for different values of  $t_L$  in two cases in which different values of the uncertainties are considered on two parameters,  $m$  and  $l_{01}$ .  $e_{pL}$  does not always decrease when  $t_L$  increases.

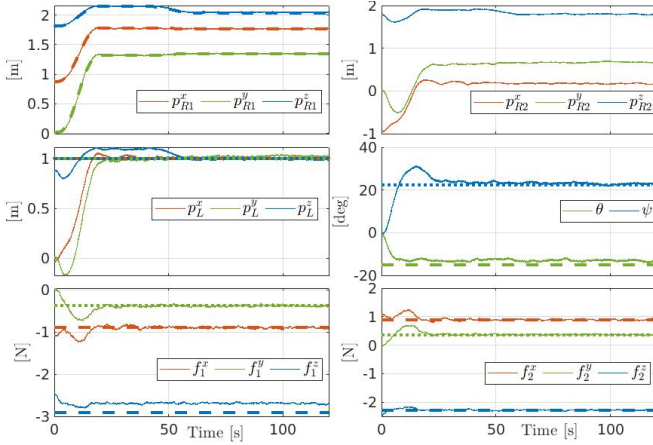


Fig. 11: Simulation results for  $t_L = 1$  N and a 5% error on each parameter. Around Time = 41 s, the leader robot has already completed his reference trajectory, reads the load position error, and corrects its own reference position in order to zeroing the load position error. Dotted lines of the same color indicate the corresponding desired quantities.

results, simulations have been carried out also for this case, using the Matlab-Simulink simulator used in [31]. In that simulator, the cables are modeled as mass-less extensible elements and the force is directly retrieved by the model of the cable without resorting to a wrench observer. Nevertheless, underactuated quadrotors are still considered, as well as the same trajectory controller. The results of two simulations can be found in Figure 9. Even though the load has been initialized in the desired configuration, with position  $\bar{p}_L = [0 \ 0 \ 1]^T$  and the same desired yaw and pitch as before, it moves to the vertical equilibrium, with the leader on top when  $\xi > 0$ , and the follower on top when  $\xi < 0$ , as explained by the stability analysis in Sec. IV.

4) *Position Error*: First, we provide in Fig. 10 two examples of the different behavior of  $e_{pL}$  when  $t_L$  increases and different values of the uncertainties are present. This fully supports the finding that the load position error at the equilibrium does not necessarily decrease when  $t_L$  is increased.

Anyway, as we have seen from the theory, it is possible to correct the error of the load position by acting solely on the leader robot reference position. This, in turn, does not affect the regulation of the load attitude. In Fig. 11, we report the

results of a Gazebo simulation in which the initial and desired load pose are as in Sec. VI-1,  $t_L = 1$  N, and an error equal to 5% of the nominal value is considered on each uncertain parameter. After 41 s, the leader robot corrects its reference position based on the position of the load according to (44). The results show that, consequently, the load is steered to the desired position when the new equilibrium is reached. On the other hand, as expected from the theory (see Eq. (11) and (12)), due to the inaccurate knowledge of the system parameters, the value of the pitch angle and the leader robot's cable force at the equilibrium do not match the desired values. Also, as predicted, one can observe in Fig. 11 that their values are not affected by the change in the leader robot position.

## VII. CONCLUSIONS

This work concerns the decentralized cooperative manipulation of a cable-suspended load by two aerial robots in the absence of direct communication. The robots are controlled with a leader-follower scheme achieved through an admittance controller on each robot. The controllers make use of nominal system parameters that are subject to uncertainty. The equilibrium points and their stability are formally studied. The theory demonstrates how an internal force that tends to stretch the load longitudinally, generated by non-vertically-operated cables, is beneficial in terms of stability of the load pose control as well as in terms of robustness to the uncertainties. The complete theoretical results are validated through numerical simulations embedding additional realistic effects.

In the future, an extension to non-beam-like rigid bodies manipulated by  $N > 2$  robots in the presence of uncertainties will be formally addressed, and the manipulation of deformable objects will be studied. Experimental tests outdoor could be interesting to assess the robustness of the method in windy conditions and when relying on outdoor state-estimation techniques.

## REFERENCES

- [1] A. Ollero Baturone, M. Tognon, A. Suárez Fernández-Miranda, D. Lee, and A. Franchi, "Past, present, and future of aerial robotic manipulators," 2021.
- [2] F. Ruggiero, V. Lippiello, and A. Ollero, "Aerial manipulation: A literature review," *IEEE Robotics and Automation Letters*, vol. 3, no. 3, pp. 1957–1964, 2018.
- [3] H. B. Khamseh, F. Janabi-Sharifi, and A. Abdessameud, "Aerial manipulation—a literature survey," *Robotics and Autonomous Systems*, vol. 107, pp. 221–235, 2018.
- [4] M. Tognon and A. Franchi, *Theory and Applications for Control of Aerial Robots in Physical Interaction Through Tethers*. Springer Nature, 2020, vol. 140.
- [5] M. Tognon, B. Yüksel, G. Buondonno, and A. Franchi, "Dynamic decentralized control for protocentric aerial manipulators," in *2017, Singapore, May 2017*, pp. 6375–6380.
- [6] G. Skorobogatov, C. Barrado, and E. Salami, "Multiple uav systems: A survey," *Unmanned Systems*, vol. 8, no. 02, pp. 149–169, 2020.
- [7] I. Maza, K. Kondak, M. Bernard, and A. Ollero, "Multi-UAV cooperation and control for load transportation and deployment," vol. 57, no. 1-4, pp. 417–449, 2010.
- [8] A. Mohiuddin, T. Tarek, Y. Zweiri, and D. Gan, "A survey of single and multi-uav aerial manipulation," *Unmanned Systems*, vol. 8, no. 02, pp. 119–147, 2020.
- [9] G. Loianno and V. Kumar, "Cooperative transportation using small quadrotors using monocular vision and inertial sensing," *IEEE Robotics and Automation Letters*, vol. 3, no. 2, pp. 680–687, 2017.



- [10] H.-N. Nguyen, S. Park, and D. J. Lee, "Aerial tool operation system using quadrotors as rotating thrust generators," in *2015*, Hamburg, Germany, Oct. 2015, pp. 1285–1291.
- [11] R. Ritz and R. D'Andrea, "Carrying a flexible payload with multiple flying vehicles," in *2013*, 2013, pp. 3465–3471.
- [12] F. Caccavale, G. Giglio, G. Muscio, and F. Pierri, "Cooperative impedance control for multiple uavs with a robotic arm," in *2015*, 2015, pp. 2366–2371.
- [13] S. Thapa, H. Bai, and J. Acosta, "Cooperative aerial load transport with force control," *IFAC-PapersOnLine*, vol. 51, no. 12, pp. 38–43, 2018.
- [14] K. Sreenath and V. Kumar, "Dynamics, control and planning for cooperative manipulation of payloads suspended by cables from multiple quadrotor robots," Berlin, Germany, June 2013.
- [15] C. Masone, H. H. Bühlhoff, and P. Stegagno, "Cooperative transportation of a payload using quadrotors: A reconfigurable cable-driven parallel robot," in *2016*, Oct 2016, pp. 1623–1630.
- [16] M. Manubens, D. Devaurs, L. Ros, and J. Cortés, "Motion planning for 6-D manipulation with aerial towed-cable systems," in *2013*, Berlin, Germany, May 2013.
- [17] A. Mohiuddin, Y. Zweiri, T. Taha, and D. Gan, "Energy distribution in dual-uav collaborative transportation through load sharing," *Journal of Mechanisms and Robotics*, 04 2020.
- [18] T. Lee, "Geometric control of quadrotor uavs transporting a cable-suspended rigid body," *IEEE Transactions on Control Systems Technology*, vol. 26, no. 1, pp. 255–264, 2017.
- [19] G. Li, R. Ge, and G. Loianno, "Cooperative transportation of cable suspended payloads with mavs using monocular vision and inertial sensing," *IEEE Robotics and Automation Letters*, vol. 6, no. 3, pp. 5316–5323, 2021.
- [20] D. Sanalitra, H. J. Savino, M. Tognon, J. Cortés, and A. Franchi, "Full-pose manipulation control of a cable-suspended load with multiple uavs under uncertainties," *IEEE Robotics and Automation Letters*, vol. 5, no. 2, pp. 2185–2191, 2020.
- [21] F. Rossomando, C. Rosales, J. Gimenez, L. Salinas, C. Soria, M. Sarcinelli-Filho, and R. Carelli, "Aerial load transportation with multiple quadrotors based on a kinematic controller and a neural smc dynamic compensation," *Journal of Intelligent & Robotic Systems*, vol. 100, no. 2, pp. 519–530, 2020.
- [22] V. Spurny, M. Petrlík, V. Vonasek, and M. Saska, "Cooperative transport of large objects by a pair of unmanned aerial systems using sampling-based motion planning," in *2019 24th IEEE International Conference on Emerging Technologies and Factory Automation (ETFA)*. IEEE, 2019, pp. 955–962.
- [23] P. O. Pereira and D. V. Dimarogonas, "Pose stabilization of a bar tethered to two aerial vehicles," *Automatica*, vol. 112, p. 108695, 2020.
- [24] R. C. Sundin, P. Roque, and D. V. Dimarogonas, "Decentralized model predictive control for equilibrium-based collaborative uav bar transportation," in *39th IEEE International Conference on Robotics and Automation (Accepted)*, 2022.
- [25] A. Tagliabue, M. Kamel, S. Verling, R. Siegwart, and J. Nieto, "Collaborative transportation using MAVs via passive force control," in *2017*, Singapore, 2016, pp. 5766–5773.
- [33] E. J. Smeur, de G De Croon, and Q. Chu, "Cascaded incremental nonlinear dynamic inversion for mav disturbance rejection," *Control Engineering Practice*, vol. 73, pp. 79–90, 2018.
- [26] M. Gassner, T. Cieslewski, and D. Scaramuzza, "Dynamic collaboration without communication: Vision-based cable-suspended load transport with two quadrotors," in *2017*, Singapore, May 2017, pp. 5196–5202.
- [27] D. K. D. Villa, A. S. Brandão, R. Carelli, and M. Sarcinelli-Filho, "Cooperative load transportation with two quadrotors using adaptive control," *IEEE Access*, vol. 9, pp. 129 148–129 160, 2021.
- [28] J. Fink, N. Michael, S. Kim, and V. Kumar, "Planning and control for cooperative manipulation and transportation with aerial robots," in *14th*, Lucerne, Switzerland, Sep. 2009.
- [29] D. Mellinger, M. Shomin, N. Michael, and V. Kumar, "Cooperative grasping and transport using multiple quadrotors," 2013, pp. 545–558.
- [30] A. Tagliabue, M. Kamel, R. Siegwart, and J. Nieto, "Robust collaborative object transportation using multiple mavs," *The International Journal of Robotics Research*, vol. 38, no. 9, pp. 1020–1044, 2019.
- [31] M. Tognon, C. Gabellieri, L. Pallottino, and A. Franchi, "Aerial co-manipulation with cables: The role of internal force for equilibria, stability, and passivity," , *Special Issue on Aerial Manipulation*, vol. 3, no. 3, pp. 2577 – 2583, 2018.
- [32] C. Gabellieri, M. Tognon, D. Sanalitra, L. Pallottino, and A. Franchi, "A study on force-based collaboration in swarms," *Swarm Intelligence*, vol. 14, no. 1, pp. 57–82, 2020.
- [34] M. Ryll, D. Bicego, and A. Franchi, "Modeling and control of FAST-Hex: a fully-actuated by synchronized-tilting hexarotor," in *2016*, Daejeon, South Korea, Oct. 2016, pp. 1689–1694.
- [35] J. R. Goodman, J. S. Cely, T. Beckers, and L. J. Colombo, "Geometric control for load transportation with quadrotor uavs by elastic cables," *arXiv preprint arXiv:2111.00777*, 2021.
- [36] C. Bisig, J. B. Montejo, M. R. Verbryke, A. Sathyan, and O. Ma, "Genetic fuzzy systems for decentralized, multi-uav cargo handling," in *AIAA Scitech 2020 Forum*, 2020, p. 1117.
- [37] A. Yigit, M. A. Perozo, L. Cuvillon, S. Durand, and J. Gangloff, "Novel omnidirectional aerial manipulator with elastic suspension: Dynamic control and experimental performance assessment," *IEEE Robotics and Automation Letters*, vol. 6, no. 2, pp. 612–619, 2021.
- [38] M. Ryll, G. Muscio, F. Pierri, E. Cataldi, G. Antonelli, F. Caccavale, and A. Franchi, "6D physical interaction with a fully actuated aerial robot," in *2017*, Singapore, May 2017, pp. 5190–5195.
- [39] R. Horst, P. M. Pardalos, and N. V. Thoai, *Introduction to global optimization*. Springer Science & Business Media, 2000.
- [40] H. K. Khalil and J. W. Grizzle, *Nonlinear systems*. Prentice hall Upper Saddle River, NJ, 2002, vol. 3.
- [41] A. S. Aghdam, M. B. Menhaj, F. Barazandeh, and F. Abdollahi, "Cooperative load transport with movable load center of mass using multiple quadrotor uavs," in *2016 4th International Conference on Control, Instrumentation, and Automation (ICCIA)*. IEEE, 2016, pp. 23–27.
- [42] T. Lee, M. Leoky, and N. H. McClamroch, "Geometric tracking control of a quadrotor UAV on SE(3)," in *49th*, Atlanta, GA, Dec. 2010, pp. 5420–5425.
- [43] M. Ryll, G. Muscio, F. Pierri, E. Cataldi, G. Antonelli, F. Caccavale, D. Bicego, and A. Franchi, "6D interaction control with aerial robots: The flying end-effector paradigm," vol. 38, no. 9, pp. 1045–1062, 2019.